Computers and Concrete, *Vol. 26, No. 3* (*2020*) *239-255*
DOI: https://doi.org/10.12989/cac.2020.26.3.239

Numerical simulation and experimental investigation of the shear mechanical behaviors of non-persistent joint in new shear test condition

Dandan Wang[1,2], Guang Zhang[1], Vahab Sarfarazi[3], Hadi Haeri*[4] and A.A. Naderi[3]

[1]*School of Resources and Environmental Engineering, Wuhan University of Technology, Wuhan, Hubei Province, China*
[2]*Poly Xinlian Blasting Engineering Limited Corp., Guiyang, Guizhou Province, China*
[3]*Department of Mining Engineering, Hamedan University of Technology, Hamedan, Iran*
[4]*State Key Laboratory for Deep GeoMechanics and Underground Engineering, Beijing, 100083, China*

(*Received April 5, 2020, Revised June 15, 2020, Accepted August 21, 2020*)

Abstract. Experimental and discrete element method were used to investigate the effects of joint number and its angularities on the shear behaviour of joint's bridge area. A new shear test condition was used to model the gypsum cracks under shear loading. Gypsum samples with dimension of 120 mm×100 mm×50 mm were prepared. the length of joints was 2cm. in experimental tests, the joint number is 1, 2 and 3 and its angularities change from 0° to 90° with increment of 45°. Assuming a plane strain condition, special rectangular models are prepared with dimension of 120 mm×100 mm. similar to joints configuration in experimental test, 9 models with different joint number and joint angularities were prepared. This testing show that the failure process is mostly governed by the joint number and joint angularities. The shear strengths of the specimens are related to the fracture pattern and failure mechanism of the discontinuities. The shear behaviour of discontinuities is related to the number of induced tensile cracks which are increased by increasing the rock bridge length. The strength of samples decreases by increasing the joint number and joint angularities. Failure pattern and failure strength are similar in both of the experimental test and numerical simulation.

Keywords: new shear test condition; joint number; joint angularities; discrete element method

1. Introduction

The shear behavior of rock masses is usually assessed for the proper design of structures in rock engineering. The stability of rock structures is mainly affected by discontinuities such as bedding planes, faults and joints which are already existed in the rock mass (Tang *et al*. 2001, Fan *et al*. 2018, Zhang *et al*. 2013, Yang *et al*. 2016, 2017). The mechanical properties of rocks is mainly controlled by the weakness planes due to their contact properties and forces at the interaction surfaces (Cao *et al*. 2015, Wang *et al*. 2017). For example, new cracks may get initiated from the tips of the existing joints under various loading conditions. They may continue their propagation till coalesce with the neighboring cracks, joints or surfaces. This fracture propagation mechanism may lead to the degradation of the rocks mechanical properties. The higher order displacement discontinuity method (HODDM) which is a modified indirect boundary element method have also been used for crack analyses in rock and rock-like materials. Haeri *et al.* (2014) studied the crack propagation in rock like Brazilian disc specimens containing cracks under compression. Fatehi Marji (1997, 2013) investigated the cracks propagation in rock fragmentation process and brittle materials using the modified higher order displacement discontinuity method. Experimental and numerical simulation (with HODDM) of fracture analyses and micro-crack coalescence mechanism in rock-like materials and concretes have been carried out by Haeri, Khallo and Marji (2015a, 2015b). Hosseni-nasab and Fatehi Marji (2007) developed a semi-infinite higher-order displacement discontinuity method for quasi-static analysis of radial cracks produced by blasting in a jointed rock mass. The effects of discontinuities such as joints on the failure process of a rock mass provides a valuable guiding framework for the design of actual engineering rock structures. Some researchers such as Bobet *et al*. (1998) performed some valuable experimental and numerical simulations to study the mechanical behavior of non-persistent jointed rock mass. They visualized five distinguishable failure patterns for gypsum specimens containing parallel flaws under uniaxial compressive loading condition. Some experimental works also performed by Wong *et al*. (1998) on plaster specimens under uniaxial compression and identified nine types of coalescence patterns. The jointed rock-like specimens under uniaxial compression are also studied by Cao *et al*. (2016). They investigated the ultimate uniaxial compressive strength of these materials and classified four types of the failure patterns through similar testing and numerical simulation technics. Effects of joint geometry parameters on the mechanical properties, compressive strength and failure patterns of the rock mass have been studied by Bahaaddini *et al.* (2013) using the particle flow modelling technic. The relationship between time-dependent cracks coalescence

*Corresponding author, Assistant Professor
E-mail: haerihadi@gmail.com

ISSN: 1598-8198 (Print), 1598-818X (Online)

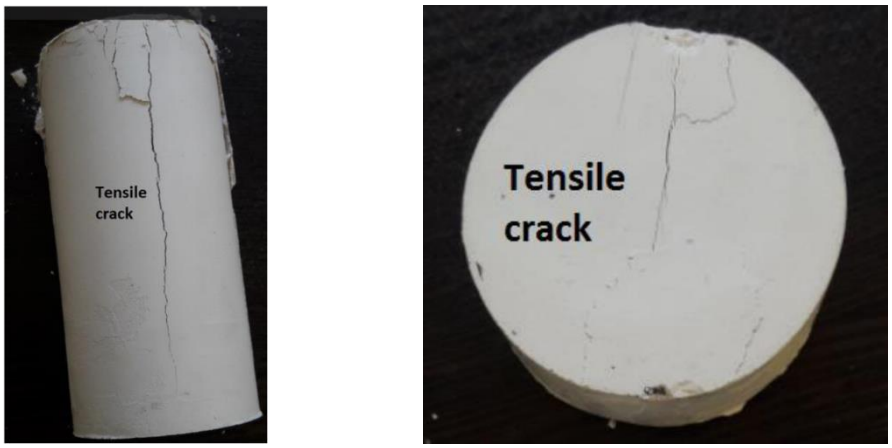

(a) (b)

Fig. 1 (a) Failure pattern in experimental compressive test, (b) failure pattern in Brazilian test

process and axial stress-time behavior for red sandstone samples containing two unparalleled cracks have been investigated by Yang *et al.* (2013) using acoustic emission and photographic monitoring technics. Effects of joint inclination angles and joint connectivity rate on the mechanical properties and strength of a rock mass containing non-persistent open joints have been studied by Chen *et al*. (2011). They conducted some uniaxial compression tests on the specially prepared gypsum specimens. The numerical simulation technic using the three dimensional particle flow code (PFC3D) has been used by Fen *et al.* (2015) to investigate the effects of multi-non-persistent joints on the mechanical behavior of jointed rock mass. The mechanical behavior of a jointed rock mass with joints adjacent to a free surface of an excavation wall is numerically simulated by Yang *et al.* (2015). The mechanical behaviors of joint interactions and rock bridges have been extensively studied by many researchers (Lee 2011, Park 2010, Ghazvinian *et al*. 2012, Nabil *et al*. 2012, Ramadoss and Nagamani 2013, Haeri *et al*. 2013, Pan *et al*. 2014, Haeri *et al*. 2015, Sarfarazi *et al*. 2014, 2016a, 2016b, 2016c, Haeri 2015, Kequan and Zhou *et al.* 2015, Yaylac 2016, Haeri *et al*. 2016a, b, c, d, Monfared *et al*. 2017, Mo and Monfared 2017, Rezaiee-Pajand *et al*. 2018, Lee and Lee 2018, Boumaaza 2017). The rock fracturing and cracks coalescence behavior of rock-like specimens (rectangular shaped) containing two parallel open cracks have been investigated by Zhang *et al.* (2013, 2015) under uniaxial compression. They concluded that the inclinations of a line linking up the tips of the inner flaw and also the spacing in between the two flaws (open cracks) affected the peak strength and coalescence patterns of the rock-like specimens. Other numerical methods, such as Peridynamics (PD) (Zhou *et al*. 2016), The Extended Finite Element Method (Zhou *et al*. 2012) and General Particle Dynamics ((Zhou *et al*. 2015, Bi *et al*. 2016) have been done on the crack propagation.

On the other hands the mechanical behavior of joints interactions in a non-persistent jointed rock mass have been rarely investigated specially under shear loading conditions. In this paper, the specially designed jointed specimens of rock-like materials are being tested under shear loading conditions. The effects of joints interactions on the failure modes, the strengths and the deformation behaviors of jointed rocks are being investigated.

Table 1 Mechanical properties of specimens

Compressive strength	7.2 MPa
Tensile strength	1.3 MPa

2. Stages of laboratory tests

Some laboratory tests being conducted on the specially prepared rock-like specimens. The Brazilian disc type specimens containing internal flaws are being tested under uniaxial compression and under shear loading.

2.1 Mechanical properties of samples

To build the samples, the gypsum and water mixture was used with a ratio of 2 to 1. uniaxial and Brazilian tests were carried out on cylindrical samples and disc samples. The cylindrical samples have a diameter of 54 mm and the height of 108 mm. The disc samples have a diameter 54 and the thickness of 27 mm. Fig. 1(a) and (b) shows failure pattern in uniaxial test and Brazilian test. Table 1 shows compressive strength and tensile strength of rock like specimens.

2.2 Preparing the specimens containing non-persistent joints

The rock-like specimens containing non-persistent joints can be prepared from a mixture of gypsum and water with a ratio of 2 to 1, respectively. This mixture is poured into some typical molds. The framework of a typical mold has dimensions of 200 mm×150 mm×200 mm (Fig. 2(a)). The mold is made of fiberglass which is waterproof and the diameter of the mold will not increase during material casting. Two timbers placed at the bottom and top of the mold as shown in Fig. 2(a). A plastic fiber with dimensions of 200 mm×150 mm×100 mm put inside the frame of mold

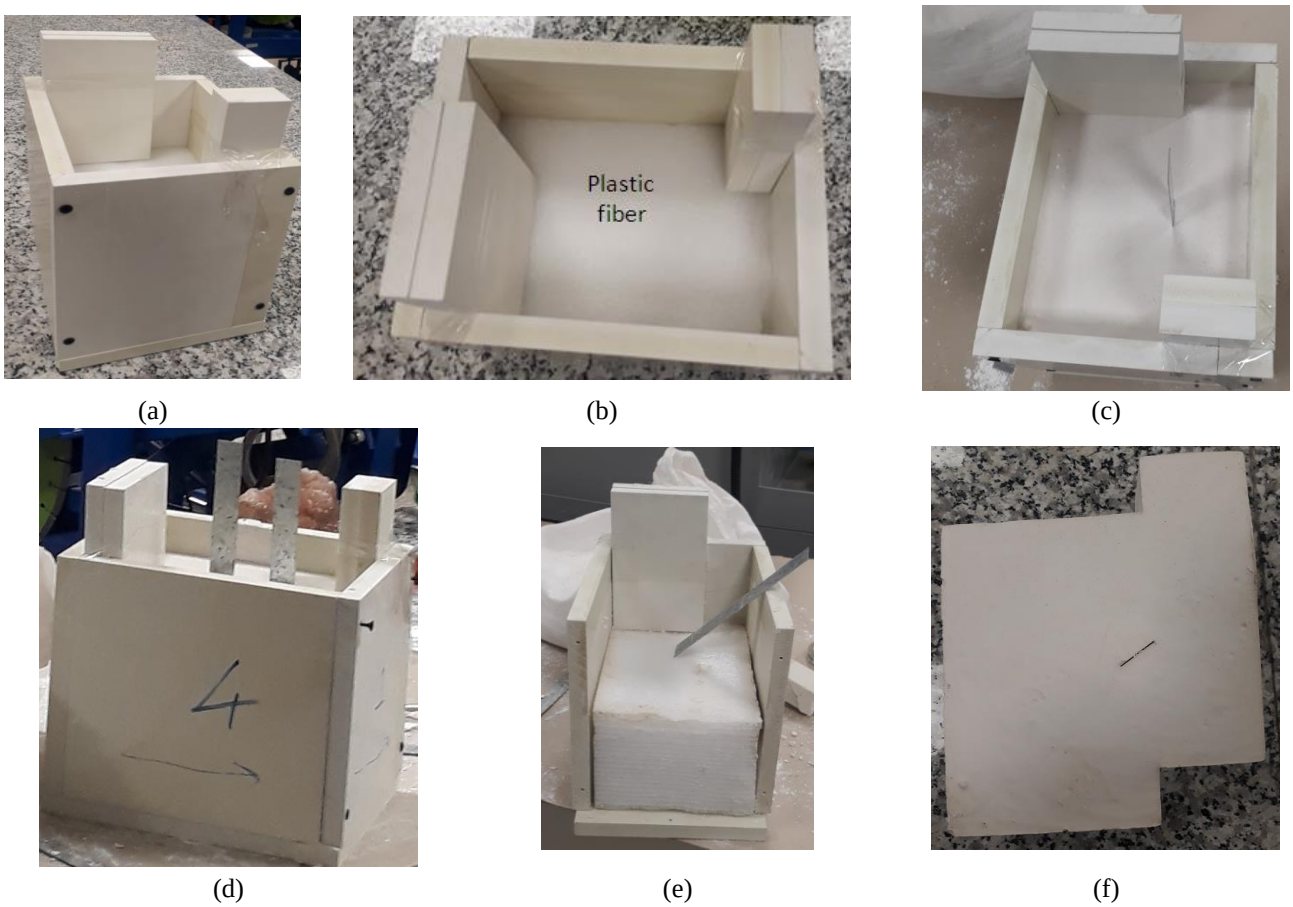

(a) (b) (c)

(d) (e) (f)

Fig. 2 (a) The frame with dimension of 200 mm×150 mm×200 mm (b) a special plastic fiber with dimension of 200 mm×150 mm×100 mm was put into the frame, (c) the shime inside the plastic fiber, (d) adjustment the shime inside the frame and plaster slurry inside the mold, (e) the aluminum sheet is removed from the mold, (f) specimen consisting non persistent joint

(a) (b) (c)

Fig. 3 (a) Joint angle is 0°, (b) joint angle is 45°, (c) joint angle is 90°

(Fig. 2(b)) and the aluminum sheets are then moved into the oil. This sheet is inserted into the plastic fiber from one side and connected to the free surface from another side of the mold (Fig. 2 (c), (d)). the blade is attached to the chalk specimen by the oil so that after removing the plaster slurry within more than 15 minutes, the aluminum sheet can be easily removed from the mold (Fig. 2(e)). The bolts of the molds are opened as shown in Fig. 2(e) so that the casted samples can be removed from the mold (Fig. 2(f)). The casted specimens can be used for the required testing after about 15 days. The test specimens containing single joint (open crack), two and more joints can be constructed by this procedure. The joint's inclinations may get different values such as 0° (Fig. 3(a)), 45° (Fig. 3(b)) and 90° (Fig. 3(c)), respectively. Nine specimens were prepared to have different joint number and inclinations.

2.3 Loading the specimen

(a) (b) (c)

Fig. 3 Continued

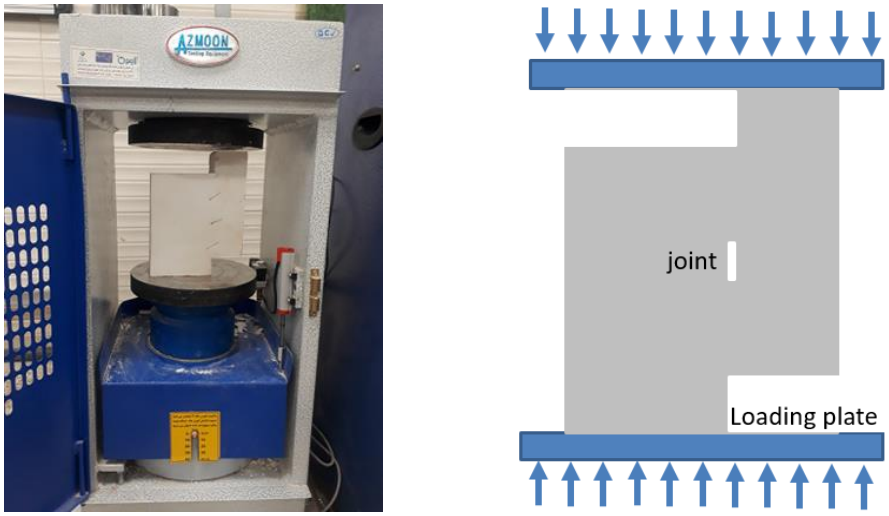

(a) (b)

Fig. 4 (a) Uniaxial machine, (b) schematic view of loading condition

In order to carry out loading on the specimens, the specimens are placed inside the uniaxial machine (Fig. 4). The loading rate was 0.005 mm/s.

3. Experimental results

3.1 Failure mechanism of samples

Fig. 5 shows the failure pattern of specimens containing non-persistent joint with joint angularity of 0°. When number of joint was 1 (Fig. 5(a)), two tensile crack initiated from joint tips and propagated parallel to loading axis till coalescence with boundaries of sample. When number of joints were 2 (Fig. 5(b)), two tensile crack initiated from the joint tips and propagated parallel to loading axis till coalescence with boundary of sample. Also two tensile cracks initiate at tip of the joints and propagate parallel to loading axis in rock bridge till coalescence with other joint tips. When number of joints were 3 (Fig. 5(c)), two tensile crack initiated from the joint tips and propagated parallel to loading axis till coalescence with boundary of sample. Also two tensile cracks initiate at tip of the joints and propagate parallel to loading axis in rock bridge till coalescence with

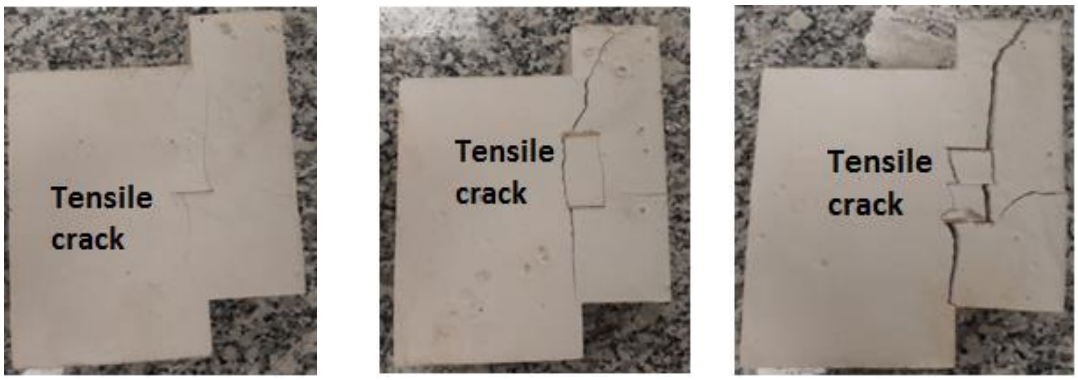

(a) (b) (c)

Fig. 5 The failure pattern in specimen with joint angularity of 0° and different joint number of ; (a) 1, (b) 2 and (c) 3

(a) (b) (c)

Fig. 6 The failure pattern in specimen with joint angularity of 45° and different joint number of (a) 1, (b) 2 and (c) 3

(a) (b) (c)

Fig. 7 The failure pattern in specimen with joint angularity of 90° and different joint number of (a) 1, (b) 2 and (c) 3

other joint tips.

Fig. 6 shows the failure pattern of specimens containing non - persistent joint with joint angularity of 45°. When number of joint was 1 (Fig. 6(a)), two tensile crack initiated from joint tips and propagated parallel to loading axis till coalescence with boundaries of sample. When number of joints were 2 (Fig. 6(b)), two tensile crack initiated from the joint tips and propagated parallel to loading axis till coalescence with sample boundaries. Also two tensile cracks initiate at tip of the joints and propagate parallel to loading axis in rock bridge till coalescence with other joint tips. When number of joints were 3 (Fig. 6(c)), two tensile crack initiated from the joint tips and propagated parallel to loading axis till coalescence with sample boundaries. Also two tensile cracks initiate at tip of the joints and propagate parallel to loading axis in rock bridge till coalescence with other joint tips.

Fig. 7 shows the failure pattern of specimens containing non - persistent joint with joint angularity of 90°. When number of joint was 1 (Fig. 7(a)), two tensile crack initiated from joint tips and propagated parallel to loading axis till coalescence with boundaries of sample. When number of joints were 2 (Fig. 7(b)), two tensile crack initiated from the joint tips and propagated parallel to loading axis till

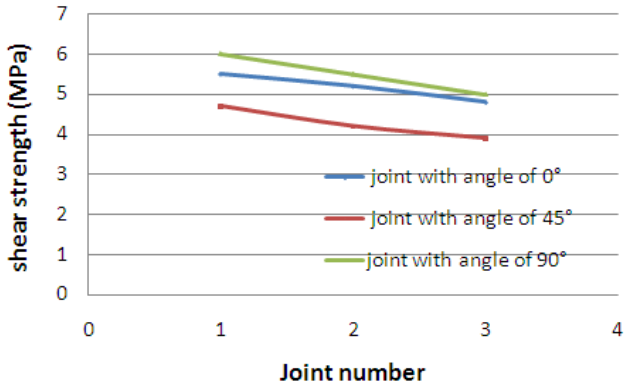

Fig 8 the effect of joint length and joint angularity on the shear strength of samples

coalescence with sample boundaries. Also two tensile cracks initiate at tip of the joints and propagate parallel to loading axis in rock bridge till coalescence with other joint tips. When number of joints were 3 (Fig. 7(c)), two tensile crack initiated from the joint tips and propagated parallel to loading axis till coalescence with sample boundaries. Also two tensile cracks initiate at tip of the joints and propagate parallel to loading axis in rock bridge till coalescence with other joint tips.

3.2 The effect of joint length on the strength of samples

Fig 8 shows the effect of joint number and joint angularity on the shear strength of samples. The strength of samples decreases by increasing the joint number. Also, joint with angle of 45° has less shear strength.

4. Numerical simulations of the laboratory tests by discrete element method

A sophisticated discrete element code known as two dimensional particle flow code (PFC2D) can be used to simulate all of the laboratory tests carried out in this study. In the numerical simulation process, the specimen is represented as an assembly of rigid particles being able to move independently and interact with one another only at the contact points (Potyondy and Cundall 2004). A central explicit finite difference scheme is implemented in the discrete element method (DEM) to compute the movements and contact forces in the particle assembly. The linear and non-linear contacts models augmented with the frictional sliding in between the particles are provided in PFC2D to model the geo-mechanical problems. In this study, the linear contact model is adopted which provides a linear elastic relation between the contact forces and relative displacements of the particles. A parallel-bond particle modelling algorithm is generated and several useful routines are provided to solve many complicated problems related to jointed rocks and rock-materials. The micro-properties of the geo-materials should be defined which are: stiffness ratios *Kn/Ks*, the ball-to ball contact modulus and coefficient of friction, the parallel normal and shear

Table 2 Micro properties used to represent the intact rock

Parameter	Value	Parameter	Value
Type of particle	disc	Stiffness ratio	2
density	3600	Particle friction coefficient	0.5
Minimum radius	0.27	Contact bond normal strength, mean (MPa)	7.8
Size ratio	1.56	Contact bond normal strength, SD (MPa)	2
Porosity ratio	0.08	Contact bond shear strength, mean (MPa)	7.8
Damping coefficient	0.7	Contact bond shear strength, SD (MPa)	2
Contact young modulus (GPa)	1		

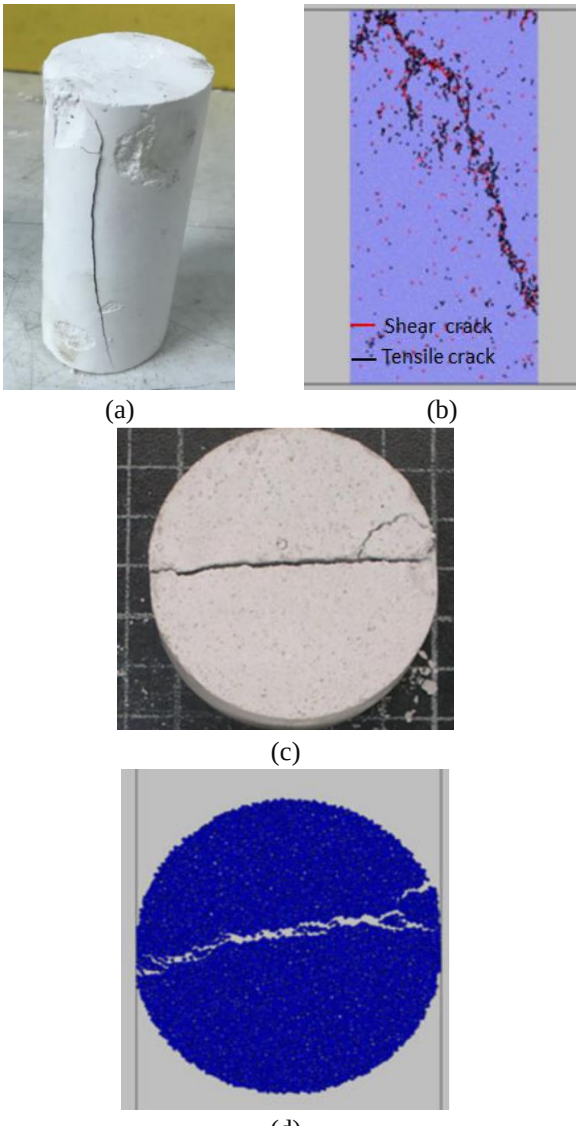

Fig. 9 (a) Experimental compression test, (b) numerical compression test, (c) experimental Brazilian test and (d) numerical Brazilian test

bonding strengths, the ratio of standard deviation to that of the mean normal and shear bonding strengths, the minimum ball radius, the radius multiplier of the parallel-bond, the parallel-bond modulus and stiffness ratio. A calibration

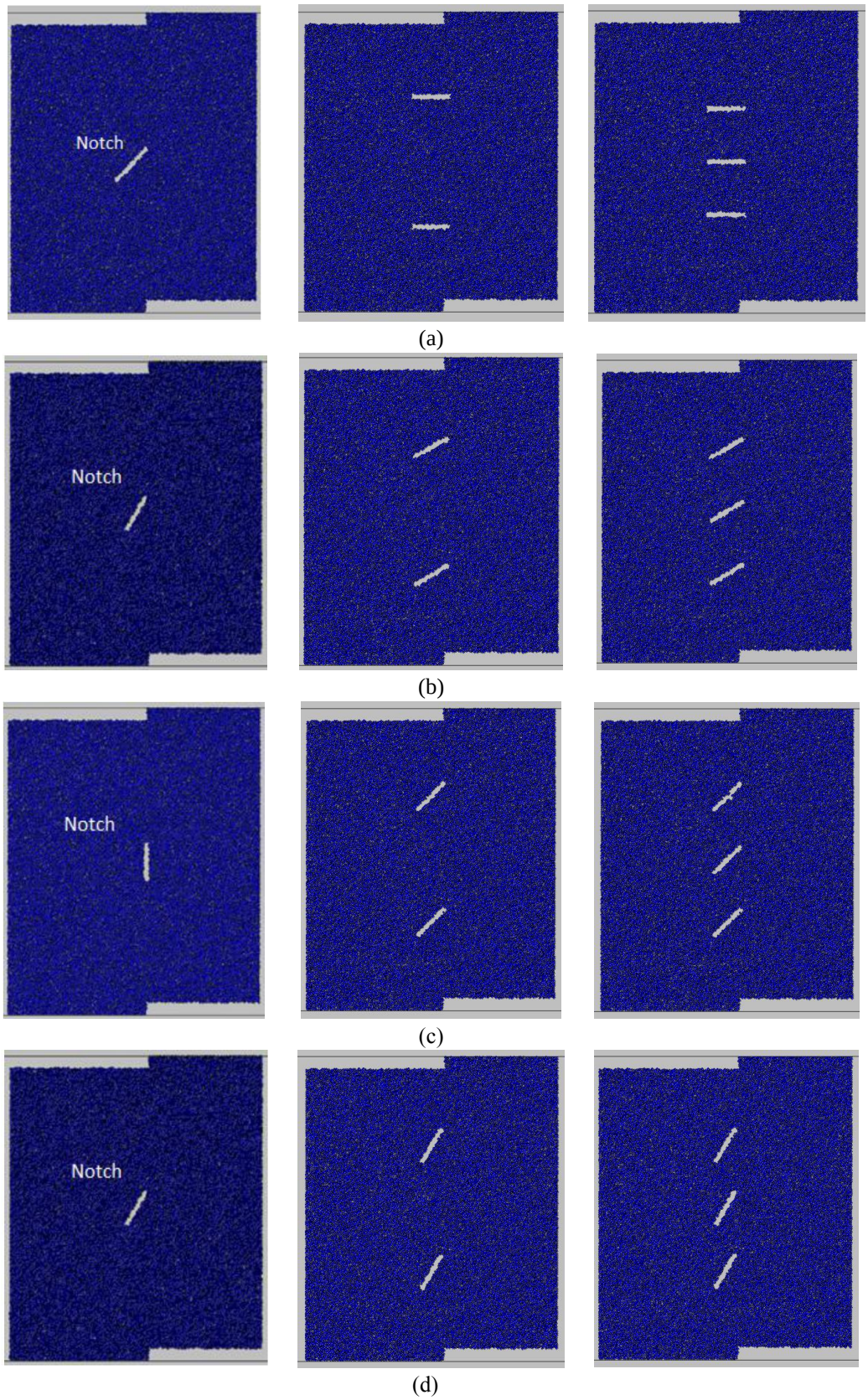

Fig. 10 (a) Joint angle is 0°, (b) joint angle is 30°, c) joint angle is 45°, d) joint angle is 60°

procedure is adopted to provide the suitable micro mechanical properties required for the particle assembly. The macro-mechanical properties gained from the laboratory modeled samples cannot be directly used for determining the bonding characteristics and contact mechanical properties. The laboratory experiments give the

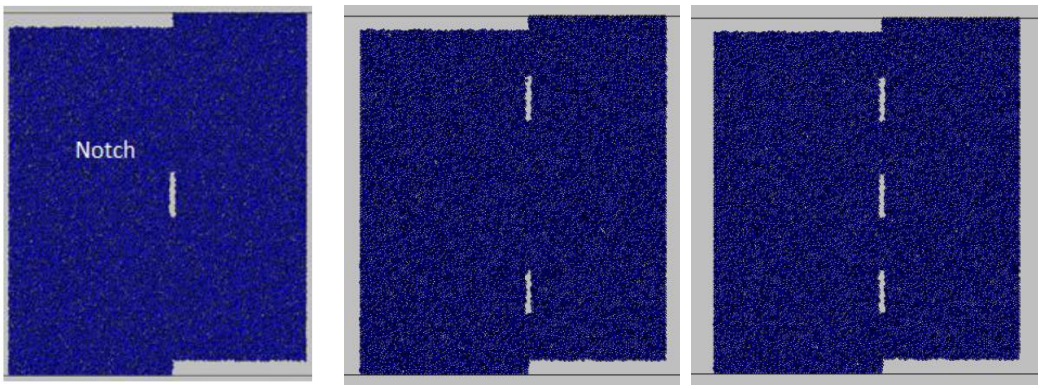

(e)

Fig. 10 Continued (e) joint angle is 90°

macro mechanical properties of the test samples and reflecting the continuum behavior of the material. Therefore, an inverse modeling procedure based on the trial and error algorithm are adopted to relate these two sets of material properties so that the suitable strengths and deformation characteristics required for the numerical modeling of the specimens can be appropriately estimated from the laboratory testing results. These estimated micro-mechanical properties for the particle assembly can be effectively used to simulate the shear behavior of non-persistent jointed rocks.

4.1 Preparing and calibrating the numerical model

The uniaxial compression test and Brazilian test was used to calibrate the compressive strength, young modulus and tensile srength of specimen in PFC2D model. The standard process of generation of a PFC2D assembly to represent a test model involves four steps: (a) particle generation and packing the particles, (b) isotropic stress installation, (c) floating particle elimination, and (d) bond installation. Adopting the micro-properties listed in Table 2 and the standard calibration procedures (Potyondy and Cundall 2003), a calibrated PFC particle assembly was created. The dimension of the uniaxial model were 54 mm and 108mm. The specimen was made of 12,615 particles. The upper and lower walls was moved toward each other with a low speed of 0.016 m/s. The diameter of the brazilian model were 54 mm. The specimen was made of 6421 particles. The left and rigth walls was moved toward each other with a low speed of 0.016 m/s. Fig. 9 (a) and (c) shows the experimental uniaxial compression test and experimental Brazilian test, respectively. Also Fig. 9 (b) and (d) shows numerical uniaxial compression test and numerical Brazilian test, respectively. The results show well matching between experimental test and numerical simulation. The uniaxial compression strength, Young modulus and Brazilian tensile strength have been depicted in Table 3. These mechanical properties are well matching with those of experimental test (Table 1). This shows that model is calibrated correctly.

4.2 Numerical compressive tests on the non-persistent open joint

Table 3 Mechanical properties in numerical models

Uniaxial compressive strength (MPa)	7.4
Young modulus (GPa)	9.3
Tensile strength (MPa)	1.4

After calibration of PFC2D, punch shear tests for jointed rock were numerically simulated by creating a box model in the PFC2D (by using the calibrated micro-parameters) (Fig. 10). The PFC specimen had the dimensions of 100 mm×100 mm. A total of 13168 disks with a minimum radius of 0.27 mm were used to make up the box specimen. Two walls exist at the upper and lower of the model. The non-persistent joints were formed by deletion of bands of particles from the model. The opening of these notches is 1 mm (Fig. 10). In general, the models containing one, two and three joint were constructed. The joint angularities changed in five different values; i.e., 0° (Fig. 10(a)), 30° (Fig. 10(b)), 45° (Fig. 10(c)), 60° (Fig. 10(d)) and 90° (Fig. 10(e)). It should be noticed that joint configuration is similar to experimental one in three different joint configuration i.e., 0°, 45° and 90°. Upper and lower walls applied uniaxial force on the model. The compression force was registered by taking the reaction forces on the upper wall.

4.3 The modeled parallel bond forces before the crack initiation process

The parallel bond force distribution (as shown in Figs. 11-15) illustrates the state of force vectors within the modelled samples before the crack initiation process for five configuration of non-persistent joint (i.e., when joint angle is 0°, 30°, 45°, 60° and 90°). The red and dark lines shown in Figs. 11-15 represent the tensile and compression force vectors in the model, respectively. The coarse lines and their accumulation show the areas where larger forces are induced within the model. It can be easily seen that the tensile forces of the bonded particles at the tip of the crack are more than their shear strength, therefore, the tensile crack initiation is a dominant mode of fracturing that initiates at the tip of the crack within the modelled samples.

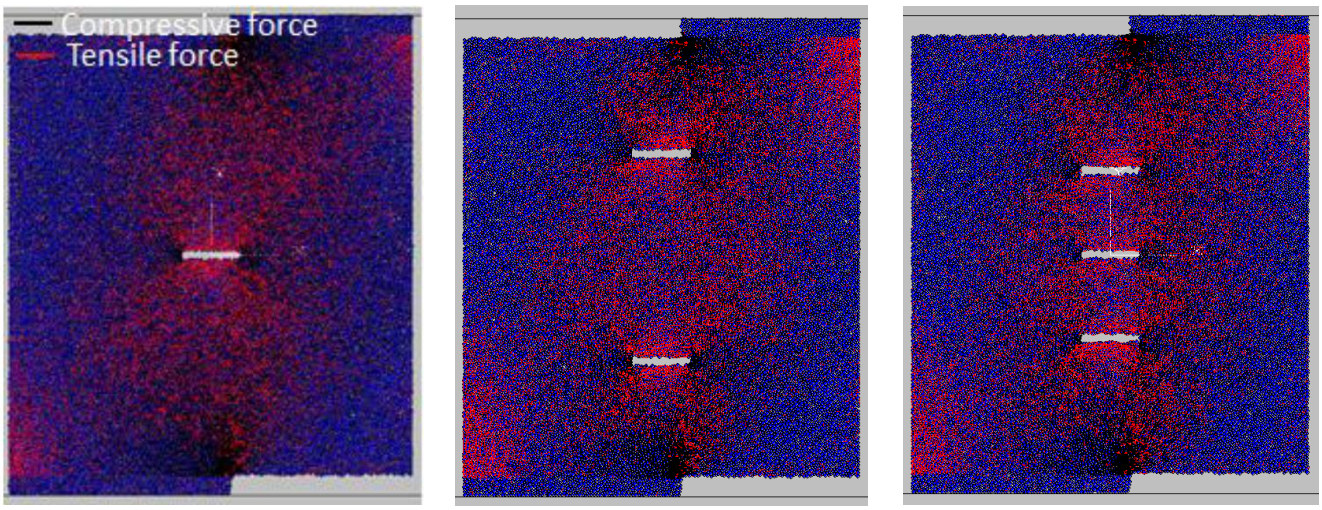

(a) (b) (c)

Fig. 11 The parallel bond force distribution in model with joint angularity of 0° and different joint number of (a) 1, (b) 2 and (c) 3

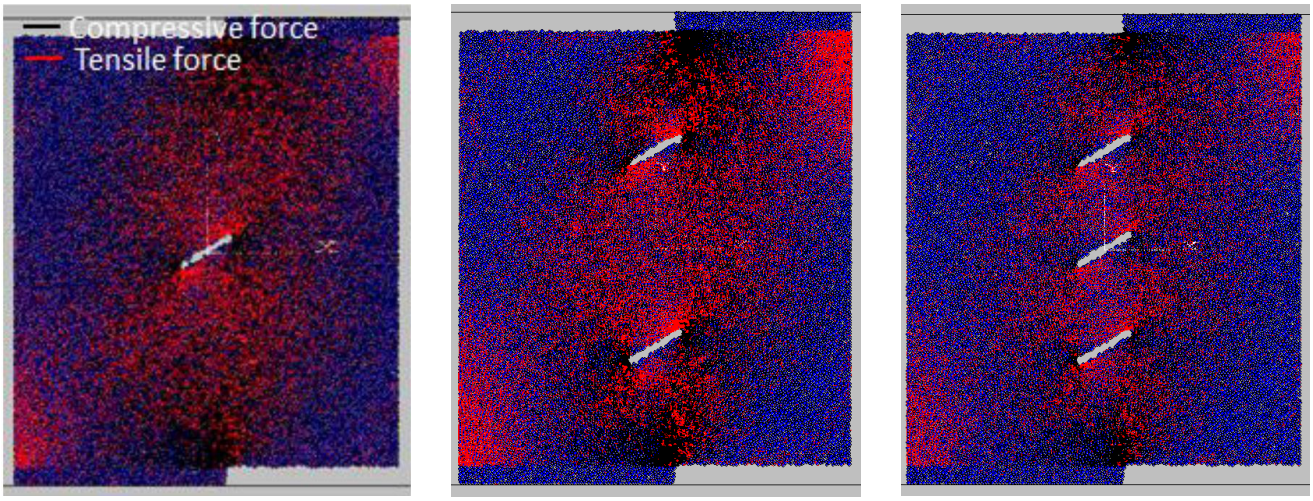

(a) (b) (c)

Fig. 12 The parallel bond force distribution in model with joint angularity of 30° and different joint number of (a) 1, (b) 2 and (c) 3

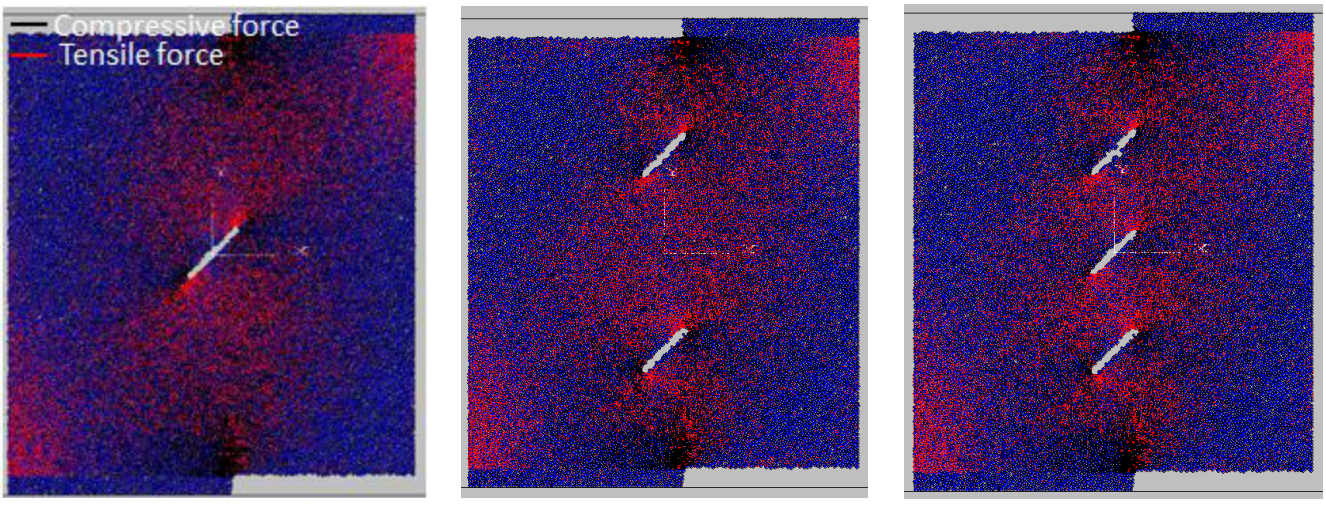

(a) (b) (c)

Fig. 13 The parallel bond force distribution in model with joint angularity of 45° and different joint number of (a) 1, (b) 2 and (c) 3

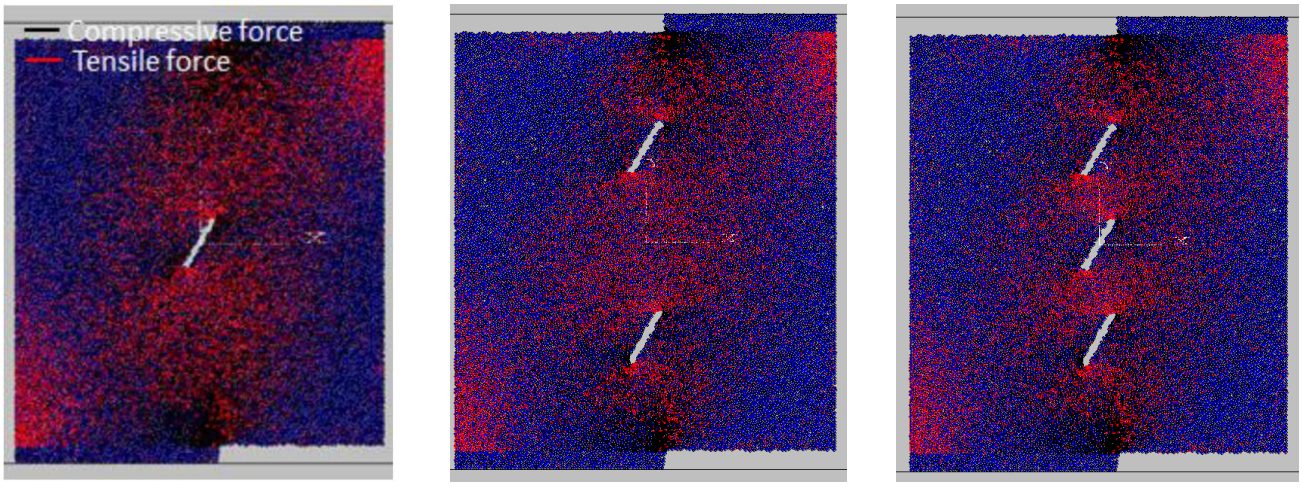

(a) (b) (c)

Fig. 14 The parallel bond force distribution in model with joint angularity of 60° and different joint number of (a) 1, (b) 2 and (c) 3

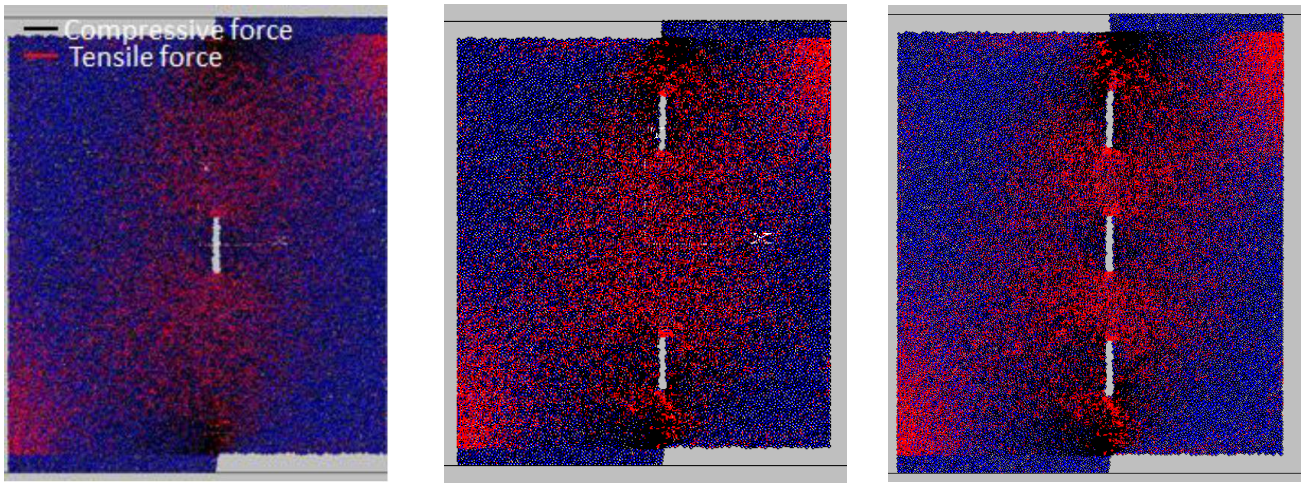

(a) (b) (c)

Fig. 15 The parallel bond force distribution in model with joint angularity of 90° and different joint number of (a) 1, (b) 2 and (c) 3

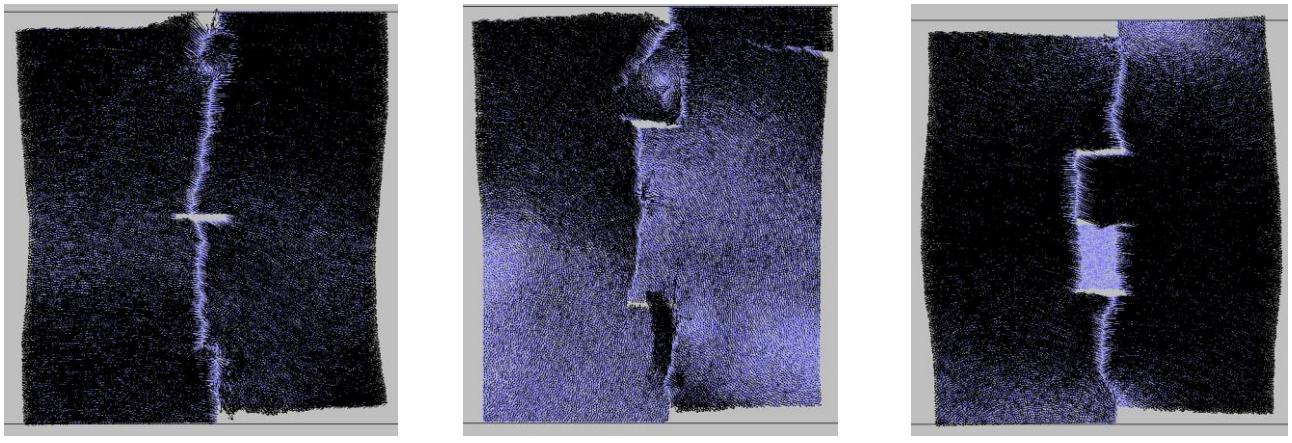

(a) (b) (c)

Fig. 16 The particle displacement vectors in model with joint angularity of 0° and different joint number of (a) 1, (b) 2 and (c) 3

4.4 The distribution of displacement vectors in the modeled samples

The distribution of particle displacement vectors in the modelled sample is shown in Figs. 16-20. The typical

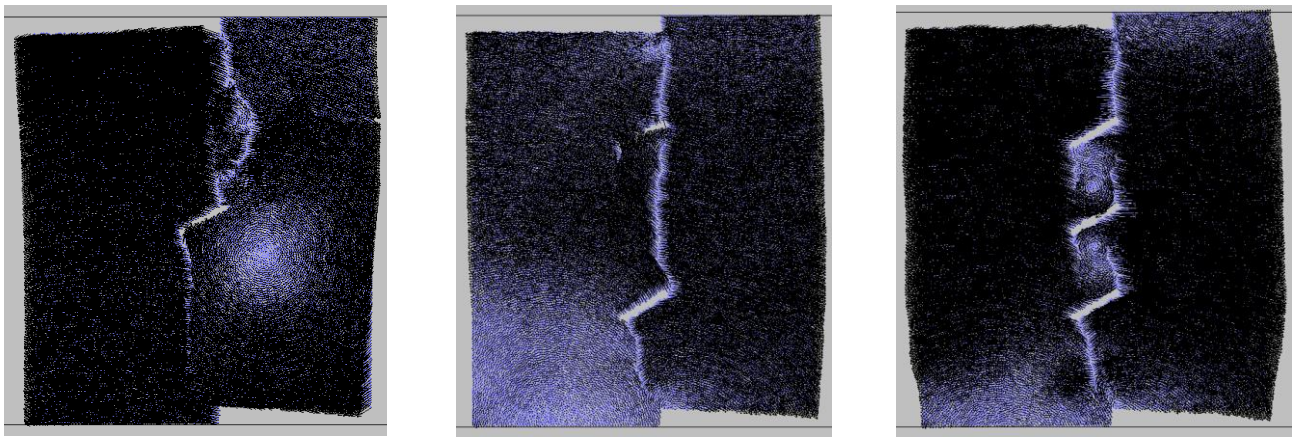

(a) (b) (c)

Fig. 17 The particle displacement vectors in model with joint angularity of 30° and different joint number of (a) 1, (b) 2 and (c) 3

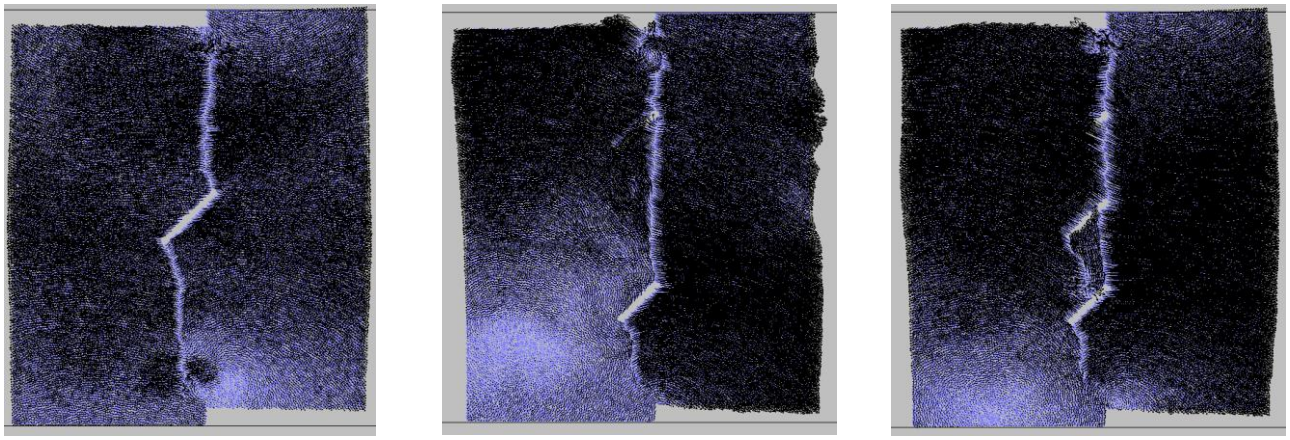

(a) (b) (c)

Fig. 18 The particle displacement vectors in model with joint angularity of 45° and different joint number of (a) 1, (b) 2 and (c) 3

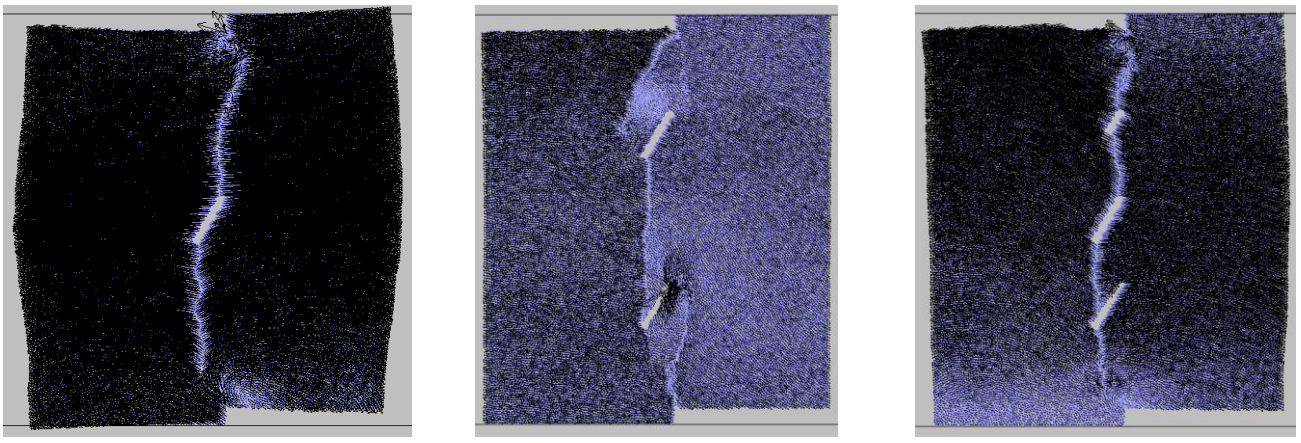

(a) (b) (c)

Fig. 19 The particle displacement vectors in model with joint angularity of 60° and different joint number of (a) 1, (b) 2 and (c) 3

displacement vector observed in the Brazilian tensile test simulation using the same micro-parameters as in the shear test is shown in Fig. 21. The displacement vectors of the particles in a modelled sample illustrate how the particles are moving as they are subjected to the external loading conditions. Figs. 16-21 illustrates that in both the shear test and the Brazilian test, the displacement vectors show similar trends, and the fractures display a tensile mode of

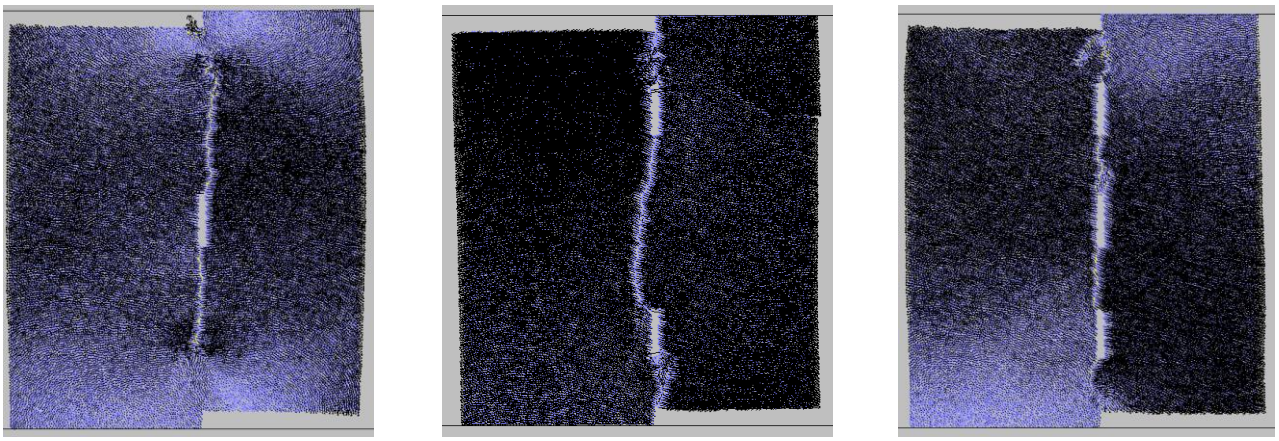

(a) (b) (c)

Fig. 20 The particle displacement vectors in model with joint angularity of 90° and different joint number of (a) 1, (b) 2 and (c) 3

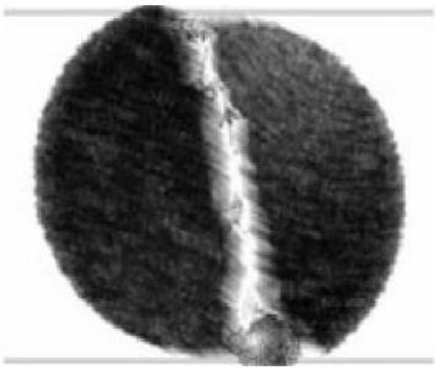

Fig. 21 The displacement vectors observed in a Brazilian tensile test

failure, characteristic of Mode I fractures (the fracture mechanics terminology for fractures subjected to tensile loading conditions).

4.5 The effects of joint configuration on the failure behavior of the modelled samples

The fracture patterns of the modelled samples with the different joint configuration are considered to study the effects of joint angularities and join number on fracturing process of the brittle materials.

a) Failure mechanism of the model with joint angularity of 0°

In the failure mechanism of the modelled sample with joint number of 1 (Fig. 22(a)), the tensile wing cracks initiate from the joint walls and propagate parallel to loading axis till coalescence with model boundary. Due to the lower tensile strength of the modelled sample the tensile cracks are the most dominant mode of failure compared to those of shear mode. When number of joint was 2 (Fig. 22(b)), two wing cracks initiated from joint tip and propagate parallel to loading axis till coalescence with model boundary. Also one tensile fracture initiates from lower joint tip and go through the rock bridge till coalescence with upper joint wall. When number of joint

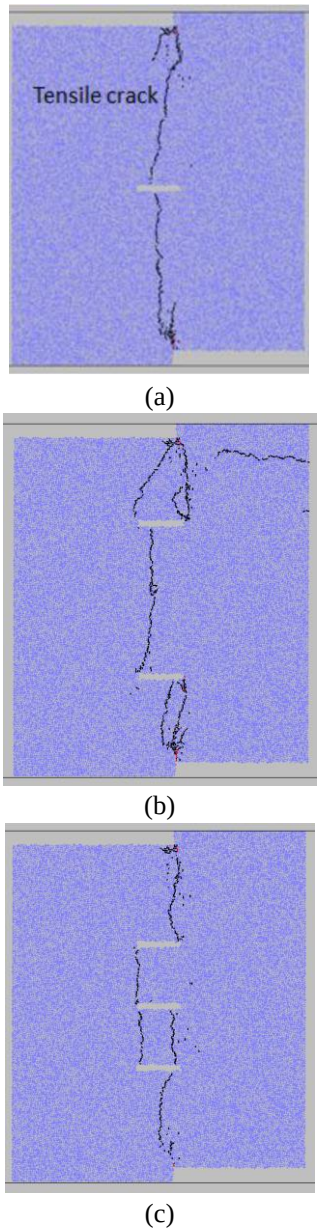

(a)

(b)

(c)

Fig. 22 The failure pattern in model with joint angularity of 0° and different joint number of (a) 1, (b) 2 and (c) 3

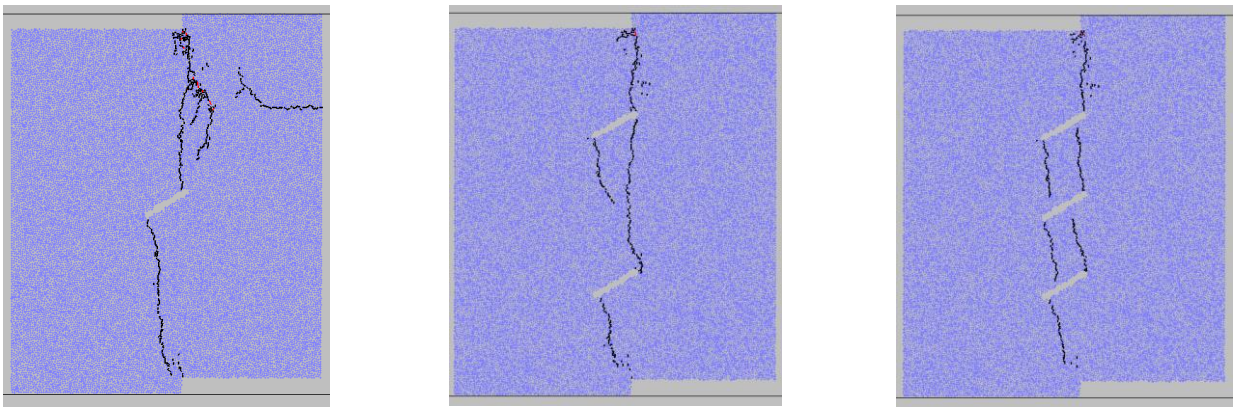

(a) (b) (c)

Fig. 23 The failure pattern in model with joint angularity of 30° and different joint number of(a) 1, (b) 2 and (c) 3

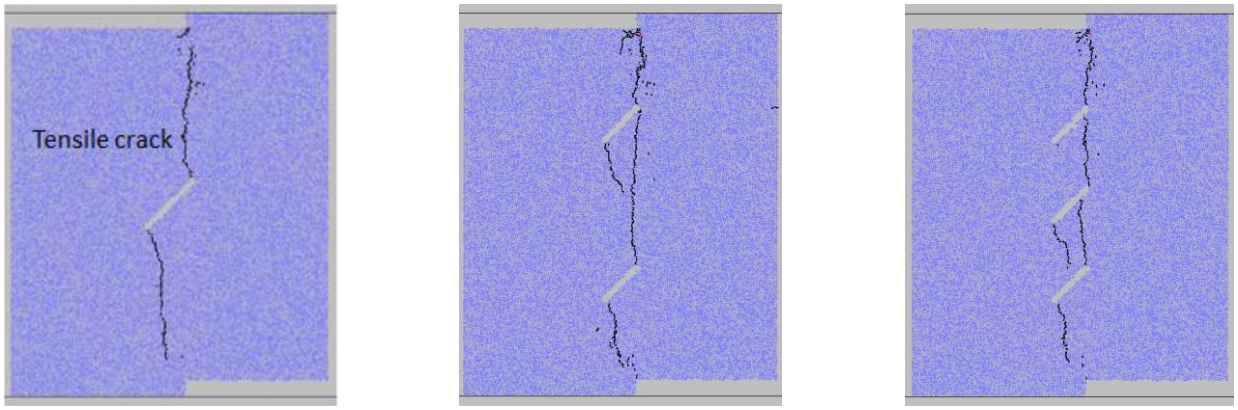

(a) (b) (c)

Fig. 24 The failure pattern in model with joint angularity of 45° and different joint number of (a) 1, (b) 2 and (c) 3

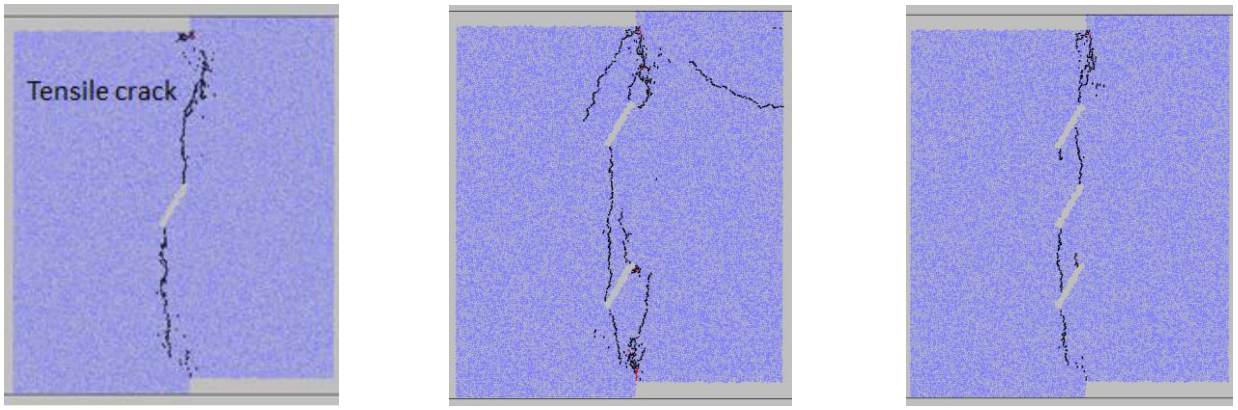

(a) (b) (c)

Fig. 25 The failure pattern in model with joint angularity of 60° and different joint number of (a) 1, (b) 2 and (c) 3

was 3 (Fig. 22(c)), two wing cracks initiated from joint tip and propagate parallel to loading axis till coalescence with model boundary. Also tensile fractures initiate from joint tips and go through the rock bridge till coalescence with other joint tips.

b) Failure mechanism of the model with joint angularity of 30°

When number of joint was 1 (Fig. 23(a)), the tensile wing cracks initiate from the joint tips and propagate parallel to loading axis till coalescence with model boundary. When number of joint was 2 (Fig. 23(b)), two wing cracks initiated from joint tip and propagate parallel to loading axis till coalescence with model boundary. Also one tensile fracture initiates from lower joint tip and go through the rock bridge till coalescence with upper joint tip. When number of joint was 3 (Fig. 23(c)), two wing cracks initiated from joint tip and propagate parallel to loading axis till coalescence with model boundary. Also tensile fractures initiate from joint tips and go through the rock bridge till

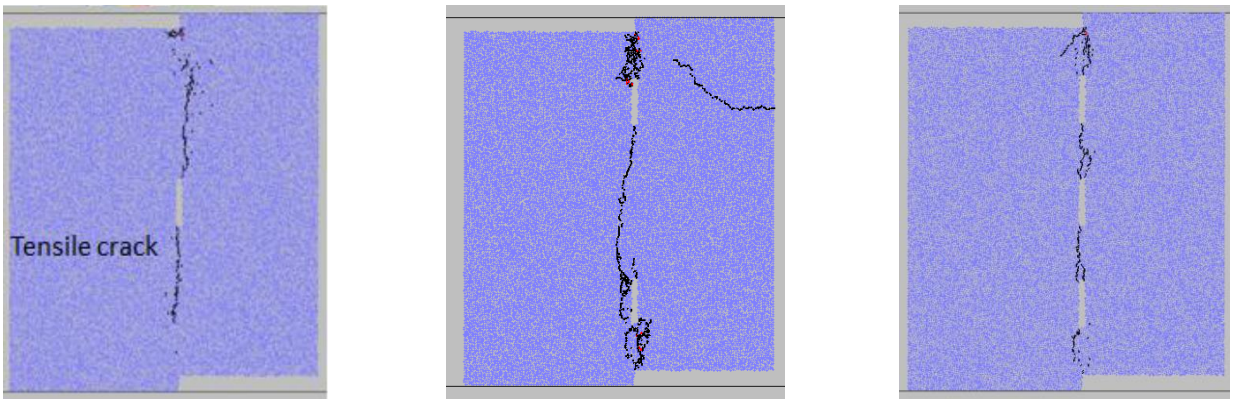

(a) (b) (c)

Fig. 26 The failure pattern in model with joint angularity of 90° and different joint number of (a) 1, (b) 2 and (c) 3

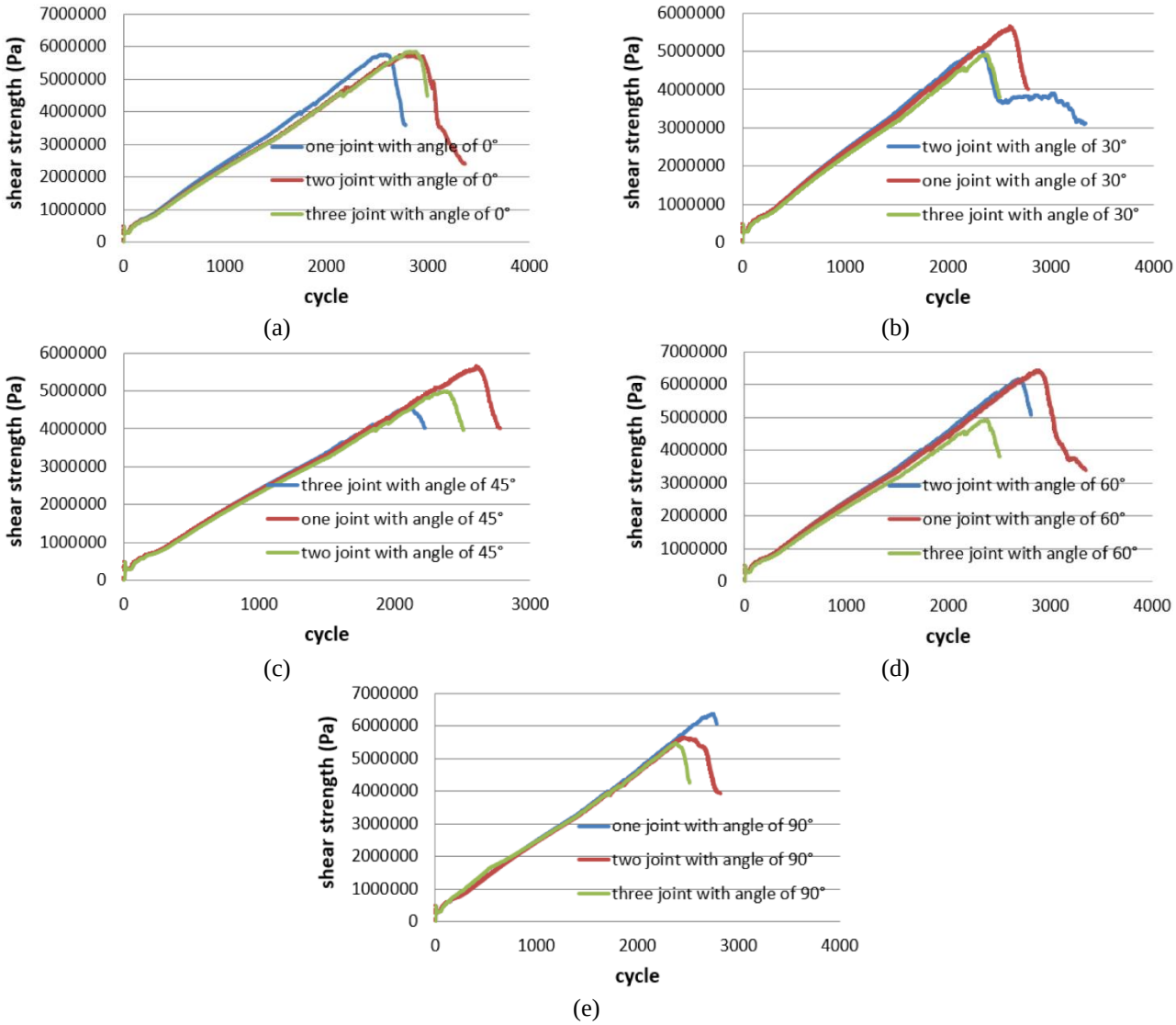

(a) (b) (c) (d) (e)

Fig. 27 The effect of joint length on the strength of models for different joint configuration; i.e., in plane parallel joint, inside echelon joint and outside echelon joint

coalescence with other joint tips.

c) Failure mechanism of the model with joint angularity of 45°

When number of joint was 1 (Fig. 24(a)), the tensile wing cracks initiate from the joint tips and propagate parallel to loading axis till coalescence with model boundary. When number of joint was 2 (Fig. 24(b)), two

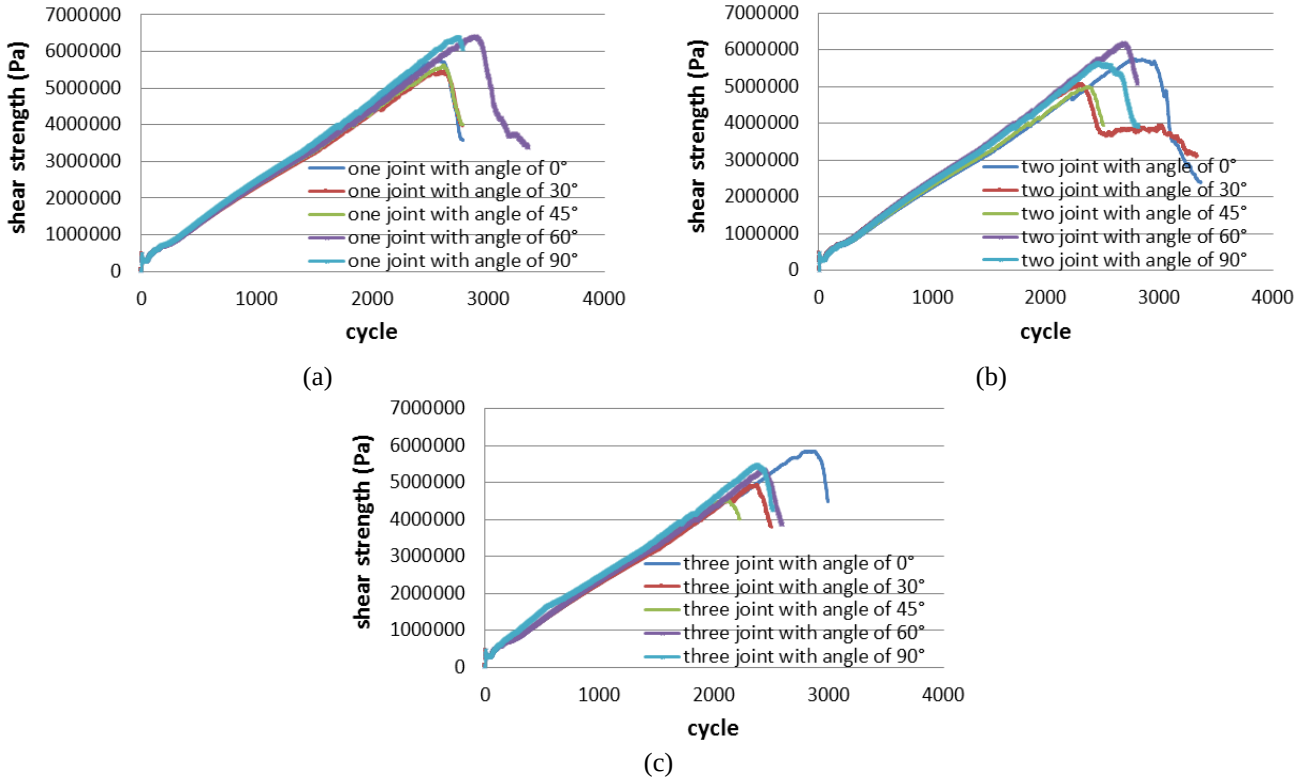

(a) (b)

(c)

Fig. 28 The effect of joint angularity on the strength of models

wing cracks initiated from joint tip and propagate parallel to loading axis till coalescence with model boundary. Also one tensile fracture initiates from lower joint tip and go through the rock bridge till coalescence with upper joint tip. When number of joint was 3 (Fig. 24(c)), two wing cracks initiated from joint tip and propagate parallel to loading axis till coalescence with model boundary. Also tensile fractures initiate from joint tips and go through the rock bridge till coalescence with other joint tips.

d) Failure mechanism of the model with joint angularity of 60°

When number of joint was 1 (Fig. 25(a)), the tensile wing cracks initiate from the joint tips and propagate parallel to loading axis till coalescence with model boundary. When number of joint was 2 (Fig. 25(b)), two wing cracks initiated from joint tip and propagate parallel to loading axis till coalescence with model boundary. Also one tensile fracture initiates from lower joint tip and go through the rock bridge till coalescence with upper joint tip. When number of joint was 3 (Fig. 25(c)), two wing cracks initiated from joint tip and propagate parallel to loading axis till coalescence with model boundary. Also tensile fractures initiate from middle joint tips and go through the rock bridge till coalescence with other joint tips.

e) Failure mechanism of the model with joint angularity of 90°

When number of joint was 1 (Fig. 26(a)), the tensile wing cracks initiate from the joint tips and propagate parallel to loading axis till coalescence with model boundary. When number of joint was 2 (Fig. 26(b)), two wing cracks initiated from joint tip and propagate parallel to loading axis till coalescence with model boundary. Also one tensile fracture initiates from lower joint tip and go through the rock bridge till coalescence with upper joint tip. When number of joint was 3 (Fig. 26(c)), two wing cracks initiated from joint tip and propagate parallel to loading axis till coalescence with model boundary. Also tensile fractures initiate from middle joint tips and go through the rock bridge till coalescence with other joint tips.

By comparison between Figs. 5-7 and Figs. 22, 24 and 26, It can be concluded that failure pattern is similar in both of the experimental test and numerical simulation.

4.6 The effect of joint numbers on the strength of samples

Fig. 27(a)-(e) shows the effect of joint number on the strength of models. When joint angle is 0°, the shear strength is constant but young modulus was decreased by increasing the joint number (Fig. 27(a)). For any other joint angularities (i.e., Fig. 27 (b)-(e)), the failure strength and young modulus decrease by increasing the joint number.

4.7 The effect of joint angularities on the strength of samples

Fig. 28(a)-(c) shows the effect of joint angularity on the strength of models. In three cases of joint number, the shear strength has minimum value when joint angles were 30° and 45°.

By comparison between Fig. 8 and Fig. 28 It can be concluded that failure strength is nearly similar in both of

the experimental test and numerical simulation.

5. Conclusions

• The tensile forces of the bonded particles at the tip of the crack are more than their shear strength, therefore, the tensile crack initiation is a dominant mode of fracturing that initiates at the tip of the crack within the modelled samples.
• in both the shear test and the Brazilian test, the displacement vectors show similar trends, and the fractures display a tensile mode of failure, characteristic of Mode I fractures (the fracture mechanics terminology for fractures subjected to tensile loading conditions).
• When number of joint was 1, the tensile wing cracks initiate from the joint tips and propagate parallel to loading axis till coalescence with model boundary. When number of joint was 2, two wing cracks initiated from joint tip and propagate parallel to loading axis till coalescence with model boundary. Also one tensile fracture initiates from lower joint tip and go through the rock bridge till coalescence with upper joint tip. When number of joint was 3, two wing cracks initiated from joint tip and propagate parallel to loading axis till coalescence with model boundary. Also tensile fractures initiate from joint tips and go through the rock bridge till coalescence with other joint tips.
• When joint angle is 0°, the shear strength is constant but young modulus was decreased by increasing the joint number. For any other joint angularities, the failure strength and young modulus decrease by increasing the joint number.
• In three cases of joint number, the shear strength has minimum value when joint angles were 30° and 45°.
• Failure pattern is similar in both of the experimental test and numerical simulation.
• Failure strength is similar in both of the experimental test and numerical simulation.

References

Bahaaddini, M., Sharrock, G. and Hebblewhite, B.K. (2013), "Numerical investigation of the effect of joint geometrical parameters on the mechanical properties of a non-persistent jointed rock mass under uniaxial compression", *Comput. Geotech.*, **49**, 206-225. https://doi.org/10.1016/j.compgeo.2012.10.012.

Bi, J., Zhou, X.P. and Qian, Q. (2016), "The 3D numerical simulation for the propagation process of multiple pre-existing flaws in rock-like materials subjected to biaxial compressive loads", *Rock Mech. Rock Eng.*, **49**(5), 1611-1627. https://doi.org/10.1007/s00603-015-0867-y.

Bobet, A. and Einstein, H.H. (1998), "Fracture coalescence in rock-type materials under uniaxial and biaxial compression", *Int. J. Rock Mech. Min. Sci.*, **35**(7), 863-888. https://doi.org/10.1016/S0148-9062(98)00005-9.

Boumaaza, M., Bezazi, A., Bouchelaghem, H., Benzennache, N., Amziane, S. and Scarpa, F. (2017), "Behavior of pre-cracked deep beams with composite materials repairs", *Struct. Eng. Mech.*, **63**(5), 575-583. http://dx.doi.org/10.12989/sem.2017.63.5.575.

Cao, P., Liu, T.Y., Pu, C.Z. and Lin, H. (2015), "Crack propagation and coalescence of brittle rock-like specimens with pre-existing cracks in compression", *Eng. Geol.*, **187**(17), 113-121. https://doi.org/10.1016/j.enggeo.2014.12.010.

Cao, R.H., Cao, P., Fan, X., Xiong, X. and Lin, H. (2016), "An experimental and numerical study on mechanical behavior of ubiquitous-joint brittle rock-like specimens under uniaxial compression", *Rock Mech. Rock Eng.*, **49**(11), 4319-4338. https://doi.org/10.1007/s00603-016-1029-6.

Chen, X., Liao, Z.H. and Li, D.J. (2011), "Experimental study of effects of joint inclination angle and connectivity rate on strength and deformation properties of rock masses under uniaxial compression", *Chin. J. Rock Mech. Eng.*, **30**(4), 781-789.

Fan, X., Kulatilake, P.H.S.W. and Chen, X. (2015), "Mechanical behavior of rock-like jointed blocks with multi-non-persistent joints under uniaxial loading: a particle mechanics approach", *Eng. Geol.*, **190**, 17-32. https://doi.org/10.1016/j.enggeo.2015.02.008.

Fan, X., Li, K., Lai, H., Xie, Y., Cao, R. and Zheng, J. (2018), "Internal stress distribution and cracking around flaws and openings of rock block under uniaxial compression: a particle mechanics approach", *Comput. Geotech.*, **102**(10), 28-38. https://doi.org/10.1016/j.compgeo.2018.06.002.

Ghazvinian, A., Sarfarazi, V., Schubert, W. and Blumel, M. (2012), "A study of the failure mechanism of planar non-persistent open joints using PFC2D", *Rock Mech. Rock Eng.*, **45**(5), 677-693. https://doi.org/10.1007/s00603-012-0233-2.

Haeri, H. (2015), "Influence of the inclined edge notches on the shear-fracture behavior in edge-notched beam specimens", *Comput. Concrete*, **16**, 605-623. http://dx.doi.org/10.12989/cac.2015.16.4.605.

Haeri, H. and Sarfarazi, V. (2016a), "The effect of micro pore on the characteristics of crack tip plastic zone in concrete", *Comput. Concrete*, **17**(1), 107-12. http://dx.doi.org/10.12989/cac.2016.17.1.107.

Haeri, H. and Sarfarazi, V. (2016b), "The effect of non-persistent joints on sliding direction of rock slopes", *Comput. Concrete*, **17**(6), 723-737. http://dx.doi.org/10.12989/cac.2016.17.6.723.

Haeri, H. and Sarfarazi, V. (2016c), "The deformable multilaminate for predicting the elasto-plastic behavior of rocks", *Comput. Concrete*, **18**, 201-214. https://doi.org/10.12989/cac.2016.18.2.201.

Haeri, H., Khaloo, A. and Fatehi Marji, M. (2015), "Fracture analyses of different preholed concrete specimens under compression", *Acta Mechanica Sinica*, **31**(6), 855-870. https://doi.org/10.1007/s10409-015-0436-3.

Haeri, H., Khaloo, A. and Marji, M.F. (2015), "Experimental and numerical simulation of the microcrack coalescence mechanism in rock-like materials", *Strength Mater.*, **47**(5), 740-754. https://doi.org/10.1007/s11223-015-9711-6.

Haeri, H., Khaloo, A. and Marji, M.F. (2015), "Fracture analyses of different pre-holed concrete specimens under compression", *Acta Mechanica Sinica*, **31**(6), 855-870. https://doi.org/10.1007/s10409-015-0436-3.

Haeri, H., Sarfarazi, V. and Lazemi, H.A. (2016d), "Experimental study of shear behavior of planar non-persistent joint", *Comput. Concrete*, **17**(5), 639-653. http://dx.doi.org/10.12989/cac.2016.17.5.649.

Haeri, H., Shahriar, K., Marji, M.F. and Moarefvand, P. (2013), "Modeling the propagation mechanism of two random micro cracks in rock Samples under uniform tensile loading", *13th International Conference on Fracture*, Beijing, China.

Haeri, H., Shahriar, K., Marji, M.F. and Moarefvand, P. (2014), "On the crack propagation analysis of rock like Brazilian disc specimens containing cracks under compressive line loading", *Lat. Am. J. Solid. Struct.*, **11**(8), 1400-1416. https://doi.org/10.1590/S1679-78252014000800007.

Hosseini Nasab, H. and Marji, M.F. (2007), "A semi-infinite higher-order displacement discontinuity method and its application to the quasistatic analysis of radial cracks produced by blasting", *J. Mech. Mater. Struct.*, **2**(3), 439-458. https://doi.org/10.2140/jomms.2007.2.439.

Kequan, Y.U. and Zhoudao, L.U. (2015), "Influence of softening curves on the residual fracture toughness of post-fire normal-strength concrete", *Comput. Concrete*, **15**(2), 102-111. https://doi.org/10.12989/cac.2015.15.2.199.

Lee, H. and Jeon, S. (2011), "An experimental and numerical study of fracture coalescence in pre-cracked specimens under uniaxial compression", *Int. J. Solid. Struct.*, **48**(6), 979-999. https://doi.org/10.1016/j.ijsolstr.2010.12.001.

Lee, J.W. and Lee, J.Y. (2018), "A transfer matrix method for in-plane bending vibrations of tapered beams with axial force and multiple edge cracks", *Struct. Eng. Mech.*, **66**(1), 125-138. https://doi.org/10.12989/sem.2018.66.1.125.

Marji, M.F. (1997), "Modelling of cracks in rock fragmentation with a higher order displacement discontinuity method", PhD Thesis, Mining Engineering (Rock Mechanics), **1**(1), 167,

Marji, M.F. (2013), "On the use of power series solution method in the crack analysis of brittle materials by indirect boundary element method", *Eng. Fract. Mech.*, **98**, 365-382. https://doi.org/10.1016/j.engfracmech.2012.11.015.

Monfared, M.M. (2017), "Mode III SIFs for interface cracks in an FGM coating-substrate system", *Struct. Eng. Mech.*, **64**(1), 71-79. https://doi.org/10.12989/sem.2017.64.1.071.

Nabil, B., Abdelkader, B., Miloud, A. and Noureddine, B. (2012), "On the mixed-mode crack propagation in FGMs plates: comparison of different criteria", *Struct. Eng. Mech.*, **61**(3), 201-213. https://doi.org/10.12989/sem.2017.61.3.371.

Pan, B., Gao, Y. and Zhong, Y. (2014), "Theoretical analysis of overlay resisting crack propagation in old cement concrete pavement", *Struct. Eng. Mech.*, **52**(4) 167-181. http://dx.doi.org/10.12989/sem.2014.52.4.829.

Park, C.H. and Bobet, A. (2010), "Crack initiation, propagation and coalescence from frictional flaws in uniaxial compression", *Eng. Fract. Mech.*, **77**(14), 2727-2748. https://doi.org/10.1016/j.engfracmech.2010.06.027.

Potyondy, D. and Cundall, P. (2004), "A bonded-particle model for rock", *Int. J. Rock Mech. Min. Sci. Geomech. Abstr.*, **41**, 1329-1364. https://doi.org/10.1016/j.ijrmms.2004.09.011.

Ramadoss, P. and Nagamani, K. (2013), "Stress-strain behavior and toughness of high-performance steel fiber reinforced concrete in compression", *Comput. Concrete*, **11**(2), 55-65. https://doi.org/10.12989/cac.2013.11.2.149.

Rezaiee-Pajand, M. and Gharaei-Moghaddam, N. (2018), "Two new triangular finite elements containing stable open cracks", *Struct. Eng. Mech.*, **65**(1), 99-110. https://doi.org/10.12989/sem.2018.65.1.099.

Sarfarazi, V. and Haeri, H. (2016a), "Effect of number and configuration of bridges on shear properties of sliding surface", *J. Min. Sci.*, **52**(2), 245-257. https://doi.org/10.12989/cac.2013.11.2.149.

Sarfarazi, V., Faridi, H.R., Haeri, H. and Schubert, W. (2016b), "A new approach for measurement of anisotropic tensile strength of concrete", *Adv. Concrete Constr.*, **3**(4), 269-284. http://dx.doi.org/10.12989/acc.2015.3.4.269.

Sarfarazi, V., Ghazvinian, A., Schubert, W., Blumel, M. and Nejati, H.R. (2014), "Numerical simulation of the process of fracture of Echelon rock joints", *Rock Mech. Rock Eng.*, **47**(4), 1355-1371. https://doi.org/10.1007/s00603-013-0450-3.

Sarfarazi, V., Haeri, H. and Khaloo, A. (2016c), "The effect of non-persistent joints on sliding direction of rock slopes", *Comput. Concrete*, **17**(6), 723-737. https://doi.org/10.1007/s00603-013-0450-3.

Tang, C.A., Lin, P., Wong, R.H.C. and Chau, K.T. (2001), "Analysis of crack coalescence in rock-like materials containing three flaws-part II: numerical approach", *Int. J. Rock Mech. Min. Sci.*, **38**(7), 925-939. https://doi.org/10.1016/S1365-1609(01)00065-X.

Wang, M., Cao, P., Wan, W., Zhao, Y.L., Liu, J. and Liu, J.S. (2017), "Crack growth analysis for rock-like materials with ordered multiple pre-cracks under biaxial compression", *J. Central South Univ.*, **24**(4), 866-874. https://doi.org/10.1007/s11771-017-3489-6.

Wong, R.H.C. and Chau, K.T. (1998), "Crack coalescence in a rock-like material containing two cracks", *Int. J. Rock Mech. Min. Sci.*, **35**(2), 147-164. https://doi.org/10.1007/s11771-017-3489-6.

Yang, S.Q., Liu, X.R. and Jing, H.W. (2013), "Experimental investigation on fracture coalescence behavior of red sandstone containing two unparallel fissures under uniaxial compression", *Int. J. Rock Mech. Min. Sci.*, **63**(5), 82-92. https://doi.org/10.1007/s11771-017-3489-6.

Yang, S.Q., Tian, W.L., Huang, Y.H., Ranjith, P.G. and Ju, Y. (2016), "An experimental and numerical study on cracking behavior of brittle sandstone containing two non-coplanar fissures under uniaxial compression", *Rock Mech. Rock Eng.*, **49**(4), 1497-1515. https://doi.org/10.1007/s11771-017-3489-6.

Yang, X.X., Jing, H.W., Tang, C.A. and Yang, S.Q. (2017), "Effect of parallel joint interaction on mechanical behavior of jointed rock mass models", *Int. J. Rock Mech. Min. Sci.*, **92**, 40-53. https://doi.org/10.1016/j.ijrmms.2016.12.010.

Yang, X.X., Kulatilake, P.H.S.W., Jing, H.W. and Yang, S. (2015), "Numerical simulation of a jointed rock block mechanical behavior adjacent to an underground excavation and comparison with physical model test results", *Tunnel. Underg. Space Technol.*, **50**, 129-142.

Yaylac, M. (2016), "The investigation crack problem through numerical analysis", *Struct. Eng. Mech.*, **57**(6), 1143-1156. https://doi.org/10.12989/sem.2016.57.6.1143.

Zhang, X.P. and Wong, L.N.Y. (2013), "Crack initiation, propagation and coalescence in rock-like material containing two flaws: a numerical study based on bonded-particle model approach", *Rock Mech. Rock Eng.*, **46**(5), 1001-1021. https://doi.org/10.1007/s00603-012-0323-1.

Zhang, X.P., Liu, Q.S., Wu, S.C. and Tang, X.H. (2015), "Crack coalescence between two non-parallel flaws in rock-like material under uniaxial compression", *Eng. Geol.*, **199**, 74-90. https://doi.org/10.1016/j.enggeo.2015.10.007.

Zhou, X.P. and Wang, Y. (2016) Numerical simulation of crack propagation and coalescence in pre-cracked rock-like Brazilian disks using the non-ordinary state-based peridynamics", *Int. J. Rock Mech. Min. Sci.*, **89**, 235-249.

Zhou, X.P. and Yang, H.Q. (2012), "Multiscale numerical modeling of propagation and coalescence of multiple cracks in rock masses", *Int. J. Rock Mech. Min. Sci.*, **55**, 15-27.

Zhou, X.P., Bi, J. and Qian, Q. (2015), "Numerical simulation of crack growth and coalescence in rock-like materials containing multiple pre-existing flaws", *Rock Mech. Rock Eng.*, **48**(3), 1097-1114.

CC